Available online at www.sciencedirect.com
ScienceDirect
Trans. Nonferrous Met. Soc. China 27(2017) 2239−2248
Transactions of Nonferrous Metals Society of China
www.tnmsc.cn

Effects of Na^+ doping on crystalline structure and electrochemical performances of $LiNi_{0.5}Mn_{1.5}O_4$ cathode material

Jiang-feng WANG, Dan CHEN, Wei WU, Li WANG, Guang-chuan LIANG

Key Laboratory of Special Functional Materials for Ecological Environment and Information, Ministry of Education, Institute of Power Source and Ecomaterials Science, Hebei University of Technology, Tianjin 300130, China

Received 13 June 2016; accepted 28 September 2016

Abstract: Pristine $LiNi_{0.5}Mn_{1.5}O_4$ and Na-doped $Li_{0.95}Na_{0.05}Ni_{0.5}Mn_{1.5}O_4$ cathode materials were synthesized by a simple solid-state method. The effects of Na^+ doping on the crystalline structure and electrochemical performance of $LiNi_{0.5}Mn_{1.5}O_4$ cathode material were systematically investigated. The samples were characterized by XRD, SEM, FT-IR, CV, EIS and galvanostatic charge/discharge tests. It is found that both pristine and Na-doped samples exhibit secondary agglomerates composed of well-defined octahedral primary particle, but Na^+ doping decreases the primary particle size to certain extent. Na^+ doping can effectively inhibit the formation of $Li_xNi_{1-x}O$ impurity phase, enhance the Ni/Mn disordering degree, decrease the charge-transfer resistance and accelerate the lithium ion diffusion, which are conductive to the rate capability. However, the doped Na^+ ions tend to occupy 8*a* Li sites, which forces equal amounts of Li^+ ions to occupy 16*d* octahedral sites, making the spinel framework less stable, therefore the cycling stability is not improved obviously after Na^+ doping.

Key words: cathode material; $LiNi_{0.5}Mn_{1.5}O_4$; Na^+ doping; electrochemical performance

1 Introduction

Lithium ion batteries (LIBs) have great potentials to be applied as large-scale power source for electric vehicles (EVs), hybrid electric vehicles (HEVs) and large-scale storage system of renewable energy due to their high energy density, long cycle life and environmental friendliness [1,2]. However, the lower energy density of currently commercially available LIBs using $LiCoO_2$, $LiFePO_4$ and $LiMn_2O_4$ as cathode materials seriously inhibits their large-scale application. Therefore, it is necessary to develop LIBs with higher energy density, which is determined by the cathode material.

$LiNi_{0.5}Mn_{1.5}O_4$ cathode material, first reported by AMINE et al in 1996 [3], has a high working voltage of 4.7 V (vs Li/Li^+) and a theoretical discharge capacity of 146.7 mA·h/g, thus resulting in a higher specific energy (~650 W·h/kg) than many commercialized compounds. Therefore, spinel $LiNi_{0.5}Mn_{1.5}O_4$ has attracted much interest as a promising cathode material of high specific energy LIBs for EVs applications [4,5]. In addition, the fast three-dimensional Li^+ ions diffusion pathways within the cubic lattice render a high power density [6]. However, $LiNi_{0.5}Mn_{1.5}O_4$ suffers from limited cycle life, particularly at elevated temperature, which is caused by the electrolyte degradation at high working voltage [7−9], or Mn^{2+} dissolution resulting from the disproportionation reaction of Mn^{3+} ions [10−13]. In order to resolve the above issues, various approaches such as structure and morphology controlling, surface coating and element doping have been employed. Among them, element doping is believed to be one of the most effective ways to improve the electrochemical performance of $LiNi_{0.5}Mn_{1.5}O_4$. It has been reported that the substitution of Ni/Mn by cations, such as Mo [14], Zn [15], Sm [16], Ti [17], Ru [18], Co [19] and Cr [20], could effectively eliminate the formation of rock-salt impurity phase and stabilize the disordering of Ni^{2+} and Mn^{4+} ions in the 16*d* octahedral sites of the *Fd*3*m* space group in the spinel structure [21], thus leading to the enhancement of cycling stability and rate capability. However, up to now, there is relatively little research on the substitution into

Foundation item: Project (E2015202356) supported by the Natural Science Foundation of Hebei Province, China; Project (2013009) supported by the Technology Innovation Foundation for Outstanding Youth of Hebei University, China
Corresponding author: Li WANG; Tel: +86-22-60204043; E-mail: wangli_hebut@163.com
DOI: 10.1016/S1003-6326(17)60250-4

Li sites. WANG et al [22] synthesized $Li_{1-x}Na_xNi_{0.5}Mn_{1.5}O_4$ cathode material via a co-precipitation method followed by a solid-state method and found that proper Na^+ doping could remarkably enhance the rate capability and cycling stability. However, in this work, the pristine sample $LiNi_{0.5}Mn_{1.5}O_4$ and Na-doped sample $Li_{0.95}Na_{0.05}Ni_{0.5}Mn_{1.5}O_4$ were prepared by simple solid-state method using NiO, Mn_3O_4, Li_2CO_3 and Na_2CO_3 as raw materials, and the effects of Na^+ doping on crystalline structure and electrochemical performances of $LiNi_{0.5}Mn_{1.5}O_4$ cathode material were investigated.

2 Experimental

2.1 Material synthesis

Pristine $LiNi_{0.5}Mn_{1.5}O_4$ cathode material was synthesized by solid-state method. The starting reagents Li_2CO_3, NiO and Mn_3O_4 with appropriate stoichiometry ratios were ball-milled for 1 h and fired initially at 500 °C for 5 h and then 850 °C for 8 h under air atmosphere with a heating rate of 5 °C/min. The as-obtained cathode material was labeled as LNMO. For the Na-doped sample, Na_2CO_3 was used as Na^+ source to give the final composition of $Li_{0.95}Na_{0.05}Ni_{0.5}Mn_{1.5}O_4$, which was named as LNMO-Na. To compensate for the lithium loss at high temperature, 3% (molar fraction) extra amount of lithium source was used in the experiment.

2.2 Characterization and electrochemical measurements

The crystalline structure of the samples was characterized by X-ray diffractometry (D8-FOCUS, Bruker, Germany) using Cu K_α radiation (λ=0.15406 nm) in the 2θ range of 10°−80°. The particle morphology of the materials was observed by scanning electron microscopy (Nova Nano SEM450, FEI, USA). The Ni/Mn ordering distribution in $LiNi_{0.5}Mn_{1.5}O_4$ material was identified by Fourier transformation infrared spectrometer (V80, Bruker, Germany) with a wavenumber scale of 400−700 cm^{-1}.

The fabrication of positive electrode was as follows. The as-prepared cathode materials were mixed with ethylene black and polytetrafluoroethylene (PTFE) in a mass ratio of 80:15:5. The CR2032 test coin cells were assembled using a lithium foil as the counter electrode, Celgard 2300 as the separator, and 1 mol/L $LiPF_6$ dissolved in ethylene carbonate (EC)−dimethyl carbonate (DMC)−ethyl methyl carbonate (EMC) (1:1:1, volume ratio) as the electrolyte in an argon-filled glove box. The cells were galvanostatically charged/discharged at various current densities (1*C*=147 mA/g) on a LAND CT2001A battery tester between 3.5 and 4.95 V (vs Li/Li^+). Cyclic voltammetry (CV) and electrochemical impedance spectroscopy (EIS) data were collected on a CHI660 electrochemical workstation. The CV curves were recorded in the voltage range of 3.4−5.0 V (vs Li/Li^+) at a scan rate of 5 mV/s. The impedance spectra were recorded by applying an ac amplitude of 5 mV over a frequency range from 10 mHz to 100 kHz at full-discharge state after rate capability test. All tests were carried out at room temperature.

3 Results and discussion

3.1 Structural characterization

Figure 1 displays the XRD patterns of the pristine and Na-doped samples. From Fig. 1(a), we can see that all the diffraction peaks can be indexed to the cubic spinel structure with *Fd*3*m* space group (JCPDS No. 80-2162) [23,24], which can be confirmed later from the CV curves or the charge−discharge curves with the presence of a small 4.0 V plateau. As for the pristine sample, besides the main spinel phase, there also exist three weak peaks at 2θ=37.5°, 43.5° and 63.5°, which can be ascribed to a rock-salt impurity phase ($Li_xNi_{1-x}O$) resulting from the oxygen loss during calcination at temperatures over 650 °C [25,26]. This indicates that

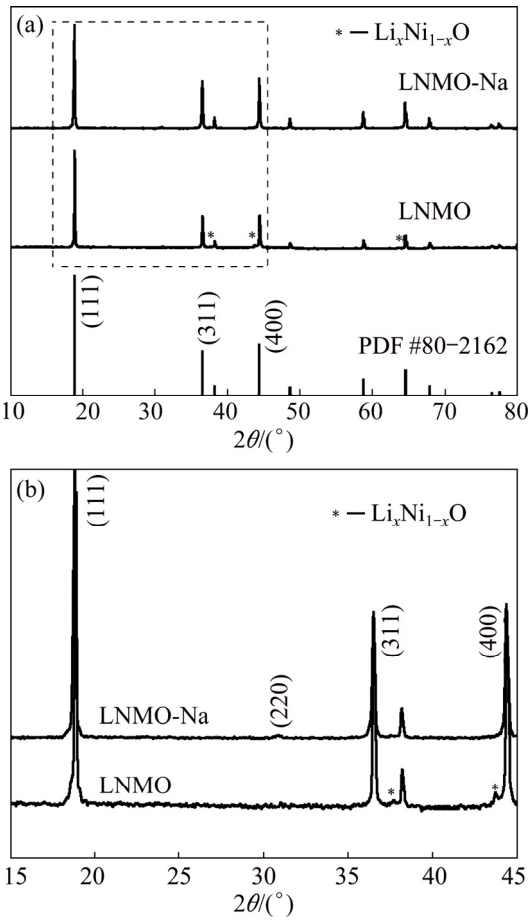

Fig. 1 XRD patterns (a) and magnification of 15°−45° (b) of pristine and Na-doped samples

part of Mn will be reduced from Mn^{4+} to Mn^{3+} in order to maintain the charge balance, thus leading to the formation of disordered phase with *Fd*3*m* space group [27]. However, the impurity phase does not exist in the Na-doped sample, indicating that the Na^+ doping can effectively inhibit the formation of rock-salt impurity phase, leading to the high phase purity of $LiNi_{0.5}Mn_{1.5}O_4$ product, which is believed to be conductive to the electrochemical performance.

From the amplified pattern between 15° and 45°, as shown in Fig. 1(b), we can see that the (111) diffraction peak of LNMO-Na shifts to lower angles compared with that of LNMO sample, which can be explained by larger ionic radius of Na^+ (1.02 Å) than that of Li^+ (0.76 Å). What's more, based on Bragg equation $2d\sin\theta=n\lambda$, we can get that the interlayer spacings of (111) lattice plane (d_{111}) for LNMO and LNMO-Na samples are 0.4706 and 0.4712 nm, respectively, as listed in Table 1, which is in consistence with the shift of (111) diffraction peak after Na^+ doping. This can further testify the successful doping of Na^+ ions into the crystal lattice. From Table 1, it can be seen that the lattice parameters and unit cell volumes of LNMO and LNMO-Na samples are 0.8163 nm, 0.5440 nm^3 and 0.8170 nm, 0.5454 nm^3, respectively. It can be seen that the Na^+ doping results in the expansion of unit cell, suggesting that Na^+ ion with larger ionic radius substituting Li^+ ion in the crystal lattice occurs. The swelling of lattice parameter will make Li^+ ion diffusion much easier, which is good for the electrochemical performance.

Table 1 Lattice parameters, d_{111}, D_{111} and I_{311}/I_{400} for pristine and Na-doped samples

Sample	a/nm	V/nm^3	d_{111}/nm	D_{111}/nm	I_{311}/I_{400}
LNMO	0.8163	0.5440	0.4706	69.28	0.948
LNMO-Na	0.8170	0.5454	0.4712	45.53	0.869

Based on Scherrer equation $D=k\lambda/\beta\cos\theta$, where k is 0.89, λ is 0.15406 nm and β is the full-width-at-half-maximum (FWHM) of the diffraction peak on a 2θ scale, we can get the crystallite size of both samples according to D_{111} value, as tabulated in Table 1. From Table 1, we can see that the D_{111} values for LNMO and LNMO-Na samples are 69.28 and 45.53 nm, respectively. It is found that Na^+ doping reduces the crystallite size, in accordance with the slightly broader diffraction peak of Na-doped sample, which is believed to be advantageous to the rate capability. This can be further verified by the following SEM observation.

From Fig. 1(b), we can also observe the presence of a weak reflection peak at ~31°, indexed as (220), in LNMO-Na sample, verifying that the Na^+ ions indeed enter into the crystal lattice and occupy part of 8*a* tetrahedral sites [28,29]. Although this will cause the expansion of unit cell, which is believed to be advantageous to the Li^+ ions diffusion, it will lead to the instability of crystal structure, which can be verified by the integrated intensity ratio of (311) to (400). It has been reported that the intensity ratio of I_{311}/I_{400} reflects the structural stability of spinel framework. The higher the I_{311}/I_{400} ratio is, the better structural stability and electrochemical performance can be achieved [30,31]. From Table 1, we know that the intensity ratio of I_{311}/I_{400} is 0.948 and 0.869, respectively, for LNMO and LNMO-Na samples, indicating that Na^+ doping is disadvantageous to the structural stability of $[Ni_{0.5}Mn_{1.5}]O_4$ spinel framework, which may be due to the weaker bonding strength of Na—O than that of Li—O. The decreased structural stability after Na^+ doping is believed to be disadvantageous to the cycling performance.

Generally, $LiNi_{0.5}Mn_{1.5}O_4$ spinel has two different crystallographic structures, depending on the oxygen stoichiometry or the ordering of Ni/Mn cations, namely, the *Fd*3*m* disordered structure, in which Ni and Mn atoms are randomly distributed in the octahedral 16*d* sites, and the $P4_332$ ordered structure, in which Ni and Mn atoms occupy the 4*a* and 12*d* octahedral sites, respectively [32,33]. However, the XRD technique could not distinguish between the two crystal structures due to the similar scattering factors of Ni and Mn [23,34]. While FT-IR spectroscopy is sensitive to the crystal symmetry, which is a useful tool to determine the structure (amorphous structure, cation ordering, etc) [34,35]. It is generally accepted that $LiNi_{0.5}Mn_{1.5}O_4$ with ordered structure in $P4_332$ space group typically produces a fingerprint spectrum consisting of eight well-defined bands [36]. Disordered phase, on the other hand, gives a rather broad spectrum with only five bands [33]. Figure 2 shows FT-IR spectra of the pristine and Na-doped samples. It can be seen that both samples have only five bands at 621, 586, 556, 505 and 475 cm^{-1}, indicating that both samples have disordered structures

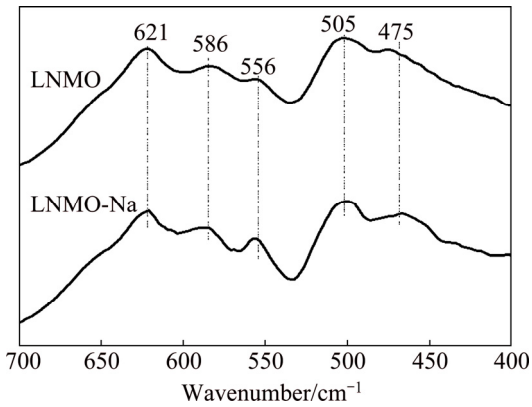

Fig. 2 FT-IR spectra of pristine and Na-doped samples

with *Fd*3*m* space group [37,38]. As reported in Refs. [39,40], the intensity ratio between the bands at 586 and 621 cm^{-1} can be used as a semiquantitative measure of the cation ordering degree in $LiNi_{0.5}Mn_{1.5}O_4$. The higher the intensity ratio is, the higher the cation ordering degree is. As Fig. 2 demonstrates, the band intensity ratios are 0.883 and 0.875 for LNMO and LNMO-Na samples, respectively, indicating that Na^+ doping increases the disordering degree of Mn and Ni in the sample, which is in consistence with the results of Ref. [22].

3.2 Morphological analysis

The structure and morphology of both $LiNi_{0.5}Mn_{1.5}O_4$ samples are illustrated in Fig. 3. It can be seen that both samples exhibit similar particle morphology, namely, secondary agglomerate composed of well-defined octahedral primary particle with smooth surface. The nonuniform particle size distribution is a characteristic of the product of solid-state method. From Fig. 3(b), we can see that despite of the existence of some large particles, the primary particle size of LNMO-Na sample is somewhat smaller than that of pristine LNMO sample, indicating that the Na^+ doping could inhibit the particle growth to some extent, in consistence with the above XRD results, which is believed to be advantageous to the rate capability. This phenomenon is consistent with, but not obviously, the finding of Ref. [22] that the particle size decreased with the increase of Na doping amount, which may be due to the different synthesis methods.

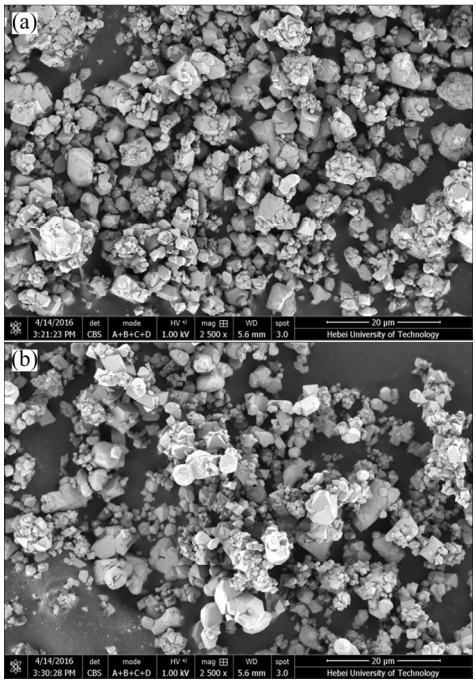

Fig. 3 SEM images of pristine and Na-doped samples: (a) LNMO; (b) LNMO-Na

3.3 Electrochemical performance

Figure 4 shows the discharge curves of the pristine and Na-doped samples at various rates of 0.2*C*, 1*C*, 5*C* and 10*C*, respectively. From Fig. 4, we can see that both samples exhibit similar discharge profiles at various rates, including a large voltage plateau at ~4.7 V and a small voltage plateau at ~4.0 V, corresponding to the Ni^{2+}/Ni^{4+} and Mn^{3+}/Mn^{4+} redox couples, respectively. The existence of small plateau at ~4.0 V confirms above structural analysis that both the pristine and Na-doped samples belong to *Fd*3*m* space group due to the disordered distribution of Ni and Mn ions in octahedral 16*d* sites.

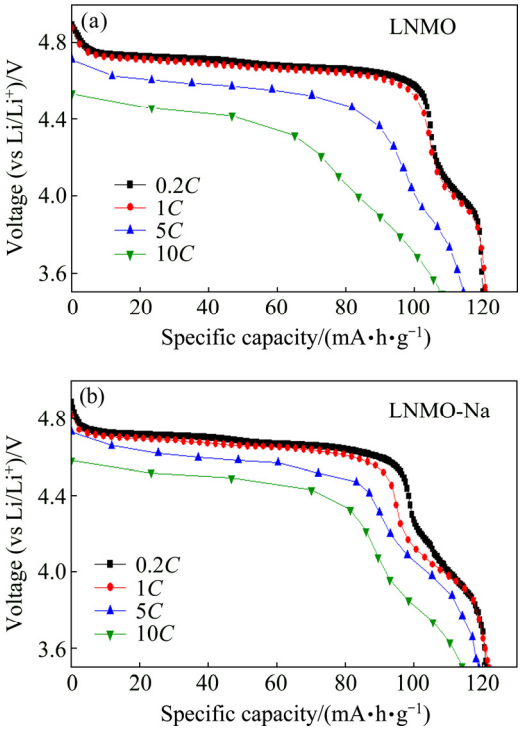

Fig. 4 Discharge curves of pristine (a) and Na-doped (b) samples at various rates

From the discharge curves at 0.2*C* rate, we can see that LNMO-Na sample has a longer voltage plateau at 4.0 V than LNMO sample, implying a higher Mn^{3+} content in Na-doped sample. It has been reported that the relative Mn^{3+} content can be directly deduced by taking the ratio of discharge capacity at plateau of 3.8−4.25 V to the total discharge capacity [29], which are 11.27% and 14.85% for LNMO and LNMO-Na samples, respectively. In theory, because of the same valence state of Na^+ with Li^+, there should not be any change in the length of 4.0 V plateau and Mn^{3+} content. The generation of Mn^{3+} is reported to be caused by two factors, that is, the formation of $Li_xNi_{1-x}O$ impurity phase and oxygen nonstoichiometry [41]. However, from the XRD patterns in Fig. 1, we can see that there is nearly no rock-salt impurity phase in LNMO-Na sample, which indicates

that there may be oxygen nonstoichiometry present in the Na-doped sample. As shown in Fig. 1(b), the weak peak at ~31° indicates that some Na^+ ions occupy the 8*a* tetrahedral sites displacing equal amounts of Li^+ ions into the 16*d* octahedral sites, and the larger Na^+ ion induces a nearby oxygen vacancy due to the compressive strain on the metal—oxygen bonds near large ions [42]. Additionally, the presence of Li^+ ions in the 16*d* octahedral sites promotes cation disordering between Mn^{4+} and Ni^{2+}. Both of the above factors lead to higher Mn^{3+} content, in other words, higher cation disordering degree in the Na-doped sample. This phenomenon is the same case as the findings of CHEMELEWSKI and MANTHIRAM [41], where parts of Ni^{2+} was substituted by Zn^{2+} with the same valence state.

From Fig. 4, we can also observe that with the discharge rate increasing, the discharge voltage plateau decreases gradually, which can be attributed to the increase in electrode over-potential and IR drop at high rates. In comparison with LNMO sample, LNMO-Na sample shows a slighter drop in the discharge voltage, implying a smaller polarization at high rates. Therefore, better rate capability can be expected for Na-doped sample. From Fig. 4, we can get that the specific discharge capacities at 0.2*C*, 1*C*, 5*C* and 10*C* rates are 119.8, 120.8, 114.2, 107.8 mA·h/g and 121.2, 121.9, 118.8, 115.1 mA·h/g, respectively, for LNMO and LNMO-Na samples, indicating that the discharge capacity at each rate, that is, the rate capability is enhanced after Na^+ doping.

In order to compare the rate capability, both samples were galvanostatically charged and discharged at room temperature at 0.2*C*, 1*C*, 5*C* and 10*C* rates and then back to 0.2*C* rate with 5 cycles per step, as illustrated in Fig. 5. We can see that the discharge capacity of LNMO-Na sample is higher than that of LNMO sample at all rates, which is more obvious at higher rates of 5*C* and 10*C*, manifesting the better rate capability of Na-doped sample. When the rate goes back to 0.2*C*, the discharge capacities of LNMO and LNMO-Na samples maintain at 121.0 and 120.0 mA·h/g, suggesting that the pristine LNMO has more stable structure compared to the Na-doped sample. This may be due to the lower bonding strength of Na—O than Li—O. The improvement of rate capability after Na^+ doping may be attributed to the following three reasons. Firstly, the Na^+ doping leads to the disappearance of rock-salt impurity phase and higher phase purity. It has been reported that the impurity would inhibit the transport of Li^+ ions in the spinel lattice, thus detrimental to the rate capability. Secondly, the Na^+ doping increases the Ni/Mn disordering degree, which can enhance the electronic conductivity by providing two additional electron hopping paths of $Ni^{2+/3+}\rightarrow Mn^{4+}\rightarrow Ni^{3+/4+}$ and $Ni^{2+/3+}\rightarrow Mn^{4+}\longleftrightarrow Mn^{3+}\rightarrow Ni^{3+/4+}$ [43], thus relieving the ohmic polarization and electrochemical polarization of materials [44], especially at higher charge/discharge rates. Thirdly, the decreased primary particle size after Na^+ doping will shorten the lithium ion diffusion distance, which is believed to be conductive to rate capability. Finally, the increase in lattice parameter and interlayer spacing after Na^+ doping enable faster Li^+ ions diffusion, which can be verified in the later EIS analysis. It is known that the Li^+ ion diffusivity is dependent on activation energy, which is closely associated with the lattice constant [45]. Because of the expansion in the lattice parameter, the Na-doped spinel structure is able to provide larger diffusion channels and hence lower activation energy to facilitate faster Li^+ ion transportation. Faster lithium mobility will give rise to better high-rate performance.

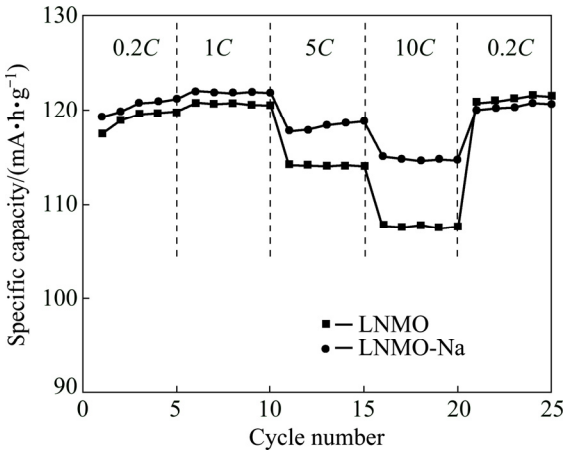

Fig. 5 Rate capability curves of pristine and Na-doped samples at various rates

Figure 6 gives the cyclic voltammograms of the pristine and Na-doped samples in the voltage range of 3.4−5.0 V (vs Li/Li^+) at a scanning rate of 5 mV/s. It can be observed that two pairs of dominant redox peaks are located in the high voltage range of 4.65−4.85 V, corresponding to the reversible reactions of the Ni^{2+}/Ni^{3+} and Ni^{3+}/Ni^{4+} couples, respectively. In addition, there also exists a pair of minor redox peaks at around 4.0 V, stemming from the redox reaction of Mn^{3+}/Mn^{4+} couple due to the oxygen deficiencies in the disordered spinel [46]. It is generally accepted that $LiNi_{0.5}Mn_{1.5}O_4$ with $P4_332$ space group shows only a strong oxidation peak around 4.7 V, but the oxidation peak splits into two separate peaks in the *Fd*3*m* spinel because the voltage difference between Ni^{2+}/Ni^{3+} and Ni^{3+}/Ni^{4+} redox couples is enhanced in the nonstoichiometric spinel [47,48]. Therefore, the observation of two oxidation peaks at around 4.7 V in Fig. 6 confirms the disordered phase with *Fd*3*m* space group for both the pristine and Na-doped samples, consistent with the FT-IR analysis. In addition, it has been reported that the peak separation

values in $LiNi_{0.5}Mn_{1.5}O_4$ samples with disordered and ordered structures are 60 and 20 mV, respectively [49,50]. From Fig. 6, we can get that the separation between the Ni redox couples is 57 and 66 mV for LNMO and LNMO-Na samples, respectively, further confirming the disordered structure of both samples. In addition, LNMO-Na sample has higher peak intensity at around 4.0 V than LNMO sample, which indicates that the Mn^{3+} content (cation disordering degree) is slightly increased after Na^+ doping, in consistence with the above FT-IR results.

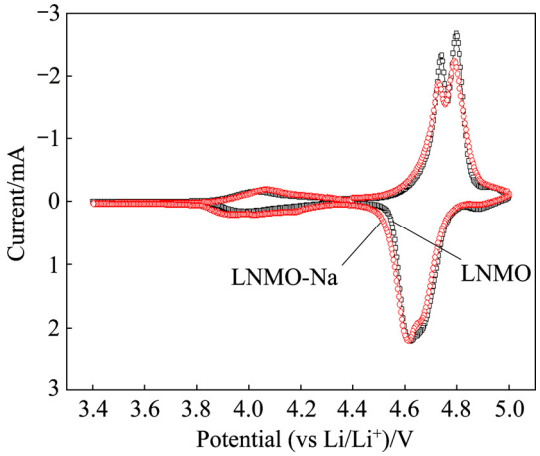

Fig. 6 Cyclic voltammograms of pristine and Na-doped samples in voltage range of 3.4−5.0 V at a scanning rate of 5 mV/s

Table 2 lists the peak values obtained from the CV curves in Fig. 6. From Table 2, we know that the potential separations ($\Delta\varphi$) between the anodic peak (φ_a) and cathodic peak (φ_c) of the Ni^{2+}/Ni^{3+} and Ni^{3+}/Ni^{4+} redox couples are 121, 131 mV and 116, 126 mV, respectively, for LNMO and LNMO-Na samples. It can be seen that the Na-doped sample has smaller potential separation values than the pristine sample, suggesting faster lithium ion insertion/extraction kinetics [51], which also accounts for the better rate capability of Na-doped sample.

Table 2 Values of CV peaks for pristine and Na-doped samples

Sample	Redox couple	φ_a/V	φ_c/V	$\Delta\varphi$/mV
LNMO	Ni^{2+}/Ni^{3+}	4.739	4.618	121
	Ni^{3+}/Ni^{4+}	4.796	4.665	131
LNMO-Na	Ni^{2+}/Ni^{3+}	4.728	4.612	116
	Ni^{3+}/Ni^{4+}	4.789	4.663	126

Figure 7 compares the cycling performance of the pristine and Na-doped samples at 1*C* rate and room temperature. From Fig. 7, we can see that the discharge capacities firstly increase in the initial several cycles and then gradually decrease with the cycling going on. The initial gradual increase of capacity is a common phenomenon, usually attributed to slow penetration of electrolyte into microparticles [52,53]. The pristine LNMO sample delivers a maximum discharge capacity of 124.0 mA·h/g and a capacity retention rate of 90.3% after 100 cycles at 1*C* rate, while LNMO-Na sample releases a higher maximum discharge capacity of 125.5 mA·h/g and a capacity retention rate of 90.7%, comparable to the pristine sample, indicating that there is little improvement in the cycling performance after Na^+ doping. This can be explained as follows. On one hand, the Na^+ doping eliminates the rock-salt impurity phase in LNMO-Na sample. It has been reported that the impurity phase will readily react with the electrolyte, therefore the elimination of impurity phase is advantageous to the cycling stability. In addition, the Na^+ doping enhances the cation disordering degree (Mn^{3+} content). The presence of Mn^{3+} has two functions. Although higher Mn^{3+} content can increase both the electronic conductivity and lithium ion diffusivity [45], it can also induce Jahn−Teller structural distortion and Mn dissolution into the electrolyte [54]. And the decreased primary particle size of Na-doped sample will increase the contact area of electrolyte with electrode material, which is also detrimental to cycling stability. On the other hand, from the XRD pattern in Fig. 1, we know that the doped Na^+ ions occupy part of 8*a* Li sites, which is believed to be disadvantageous to the structural stability of $[Ni_{0.5}Mn_{1.5}]O_4$ spinel framework. The comprehensive effect of the above factors leads to the phenomenon that the cycling performance is enhanced to little extent after Na^+ doping.

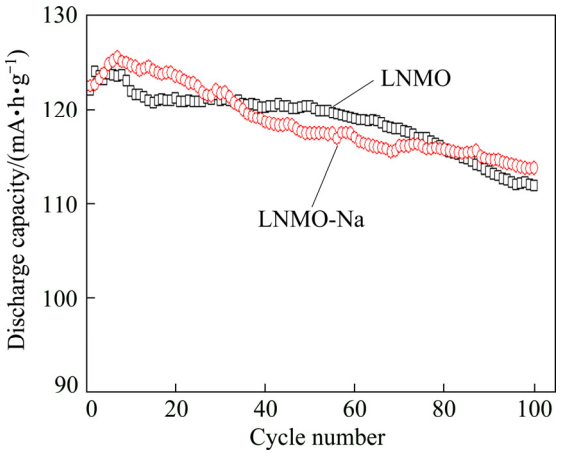

Fig. 7 Cycling performance curves of pristine and Na-doped samples at 1*C* rate

To further explore the reasons for the better electrochemical performance of LNMO-Na sample, EIS spectra were adopted on the pristine and Na-doped samples after rate capability test, as illustrated in Fig. 8(a). Both spectra have similar profiles which are

composed of a semicircle in the high-to-medium frequency region and an inclined line in the low frequency region. The semicircle is approximately related to the charge transfer process, and the inclined line is ascribed to the diffusion of lithium ions into the bulk of electrode material, the so-called Warburg diffusion. The impedance spectra can be described by the equivalent circuit presented in the inset picture, where R_e represents the electrolyte resistance, R_{ct} represents the charge transfer resistance, the Warburg element (W) represent the Warburg impedance and the constant phase element (CPE1) represents the double layer capacitance [55]. Table 3 lists the charge transfer resistance (R_{ct}) obtained by ZView software based on the equivalent circuit. It can be obviously seen that the charge transfer resistances for LNMO and LNMO-Na samples are 36.81 and 31.35 Ω, respectively, indicating that the Na-doped sample exhibits better electrochemical kinetics, which is conductive to the electrochemical performance.

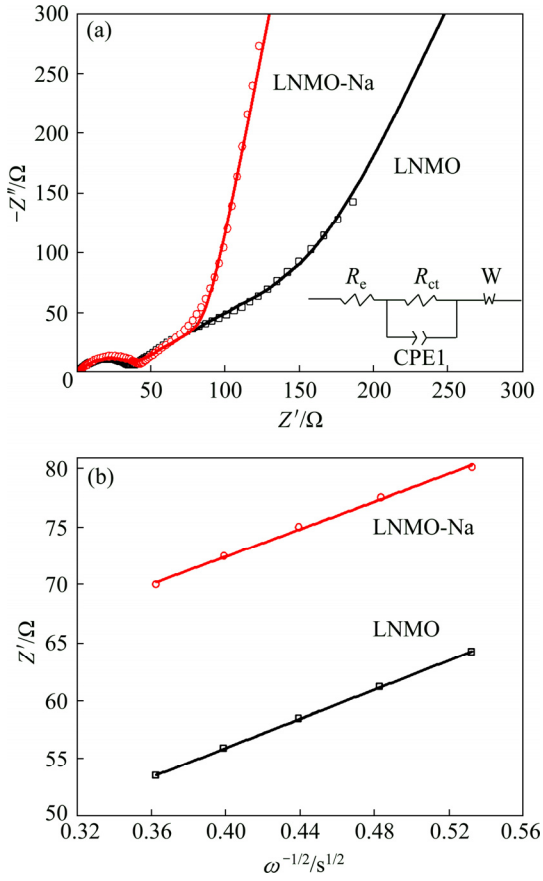

Fig. 8 Nyquist plots and fitting-curves (a) and graphs of Z' plotted against $\omega^{-1/2}$ (b) for pristine and Na-doped samples

Table 3 Charge transfer resistance (R_{ct}), σ values and Li^+ ion diffusion coefficients (D_{Li}) for pristine and Na-doped samples

Sample	R_{ct}/Ω	$\sigma/(\Omega\cdot s^{-1/2})$	$D_{Li}/(cm^2\cdot s^{-1})$
LNMO	36.81	62.798	8.807×10^{-11}
LNMO-Na	31.35	59.493	1.290×10^{-10}

Lithium ion diffusion coefficient (D_{Li}) can be roughly calculated from the following equation [56,57]:

$$D = 0.5\left(\frac{RT}{An^2F^2\sigma C}\right)^2 \quad (1)$$

where R is the gas constant (8.314 J/(mol·K)), T the temperature (298 K), A the surface area of the electrode, n the number of electrons per molecule during oxidation, F the Faraday's constant (96500 C/mol) and C the molar concentration of Li^+ ions, σ the Warburg factor which can be obtained by

$$Z' = R_e + R_{ct} + \sigma\omega^{-1/2} \quad (2)$$

where R_e is the resistance of electrolyte, R_{ct} is the charge transfer resistance and ω is the angular frequency. Both R_e and R_{ct} are independent of frequency. σ is obtained from the plot of Z' vs $\omega^{-1/2}$ (reciprocal root square of the lower angular frequencies) shown in Fig. 8(b), whose values are listed in Table 3. Based on Eq. (1), we can get that the lithium ion diffusion coefficient (D_{Li}) of LNMO-Na sample is 1.290×10^{-10} cm^2/s, higher than the value of 8.807×10^{-11} cm^2/s for LNMO sample, indicating that Na^+ doping increases the lithium ion diffusion coefficient, which can be ascribed to the absence of rock-salt impurity phase and the expansion of unit cell. The enhancement of lithium ion diffusion coefficient after Na^+ doping is in consistence with the above rate capability result.

4 Conclusions

1) SEM observations show that the pristine and Na-doped samples have similar particle morphology, but the Na^+ doping decreases the primary particle size. XRD and FT-IR analyses show that Na^+ doping does not change the *Fd*3*m* disordered structure, but increases the Ni/Mn disordering degree.

2) The rate capability is enhanced after Na^+ doping, which can be ascribed to the absence of rock-salt impurity phase, higher cation disordering degree, enlarged lattice parameters and smaller primary particle size, in consistence with the lower charge transfer resistance and higher lithium ion diffusion coefficient after Na^+ doping.

3) The cycling performance of Na-doped sample is improved to little extent in comparison with the pristine one, because the appearance of (220) weak peak in the XRD pattern implies that the doped Na^+ ions occupy part of 8*a* Li sites, which forces equal amounts of Li^+ ions to occupy the 16*d* octahedral sites, thus making the spinel framework less stable.

References

[1] PAN Cheng-chi, ZHU Yi-rong, YANG Ying-chang, HOU Hong-shuai, JING Ming-jun, SONG Wei-xin, YANG Xu-ming, JI Xiao-bo. Influences of transition metal on structural and electrochemical properties of $Li[Ni_xCo_yMn_z]O_2$ ($0.6\leq x\leq 0.8$) cathode materials for lithium-ion batteries [J]. Transactions of Nonferrous Metals Society of China, 2016, 26: 1396−1402.

[2] LUO Yun-ze, HE Li-hua, LIU Xu-heng. Effect of Mg doping on electrochemical performance of $Li_3V_2(PO_4)_3$/C cathode material for lithium ion batteries [J]. Transactions of Nonferrous Metals Society of China, 2015, 25: 2266−2271.

[3] AMINE K, TUKAMOTO H, YASUDA H, FUJITA Y. A new three-volt spinel $Li_{1+x}Mn_{1.5}Ni_{0.5}O_4$ for secondary lithium batteries [J]. Journal of the Electrochemical Society, 1996, 143: 1607−1613.

[4] GAO Zhi-gang, SUN Kai, CONG Li-na, ZHANG Yu-hang, ZHAO Qin, WANG Rong-shun, XIE Hai-ming, SUN Li-qun, SU Zhong-min. High performance 5 V $LiNi_{0.5}Mn_{1.5}O_4$ spinel cathode materials synthesized by an improved solid-state method [J]. Journal of Alloys and Compounds, 2016, 654: 257−263.

[5] ZHANG Bao, WANG Zhi-xing, GUO Hua-jun. Effect of annealing treatment on electrochemical property of $LiNi_{0.5}Mn_{1.5}O_4$ spinel [J]. Transactions of Nonferrous Metals Society of China, 2007, 17: 287−290.

[6] KANG B, CEDER G. Battery materials for ultrafast charging and discharging [J]. Nature, 2009, 458: 190−193.

[7] AURBACH D, MARKOVSKY B, SALITRA G, MARKEVICH E, TALYOSSEF Y, KOLTYPIN M, NAZAR L, ELLIS B, KOVACHEVA D. Review on electrode-electrolyte solution interactions, related to cathode materials for Li-ion batteries [J]. Journal of Power Sources, 2007, 165: 491−499.

[8] AURBACH D, MARKOVSKY B, TALYOSSEF Y, SALITRA G, KIM H J, CHOI S. Studies of cycling behavior, ageing, and interfacial reactions of $LiNi_{0.5}Mn_{1.5}O_4$ and carbon electrodes for lithium-ion 5-V cells [J]. Journal of Power Sources, 2006, 162: 780−789.

[9] KIM J H, PIECZONKA N P W, YANG Li. Challenges and approaches for high-voltage spinel lithium-ion batteries [J]. Chem Phys Chem, 2014, 15: 1940−1954.

[10] PIECZONKA N P W, LIU Zhong-yi, LU Peng, OLSON K L, MOOTE J, POWELL B R, KIM J H. Understanding transition-metal dissolution behavior in $LiNi_{0.5}Mn_{1.5}O_4$ high-voltage spinel for lithium ion batteries [J]. The Journal of Physical Chemistry C, 2013, 117: 15947−15957.

[11] JARRY A, GOTTIS S, YU Y S, ROQUE-ROSELL J, KIM C, CABANA J, KERR J, KOSTECKI R. The formation mechanism of fluorescent metal complexes at the $Li_xNi_{0.5}Mn_{1.5}O_{4-\delta}$/carbonate ester electrolyte interface [J]. Journal of the American Chemical Society, 2015, 137: 3533−3539.

[12] CHOI W, MANTHIRAM A. Comparison of metal ion dissolutions from lithium ion battery cathodes [J]. Journal of the Electrochemical Society, 2006, 153: A1760−A1764.

[13] LIN Ming-xiang, BEN Liu-bin, SUN Yang, WANG Hao, YANG Zhen-zhong, GU Lin, YU Xi-qian, YANG Xiao-qing, ZHAO Hao-fei, YU Ri-cheng, ARMAND M, HUANG Xue-jie. Insight into the atomic structure of high-voltage spinel $LiNi_{0.5}Mn_{1.5}O_4$ cathode material in the first cycle [J]. Chemistry of Materials, 2015, 27: 292−303.

[14] YI Ting-feng, CHEN Bin, ZHU Yan-rong, LI Xiao-ya, ZHU Rong-sun. Enhanced rate performance of molybdenum-doped spinel $LiNi_{0.5}Mn_{1.5}O_4$ cathode materials for lithium ion battery [J]. Journal of Power Sources, 2014, 247: 778−785.

[15] YANG Ze, JIANG Yan, KIM Jung-hyun, WU Yan, LI Guo-long, HUANG Yun-hui. The $LiZn_xNi_{0.5-x}Mn_{1.5}O_4$ spinel with improved high voltage stability for Li-ion batteries [J]. Electrochimica Acta, 2014, 117: 76−83.

[16] MO Ming-yue, HUI K S, HONG Xiao-ting, GUO Jun-sheng,YE Cheng-cong, LI Ai-ju, HU Nan-qian, HUANG Zhen-ze, JIANG Jian-hui, LIANG Jing-zhi, CHEN Hong-yu. Improved cycling and rate performance of Sm-doped $LiNi_{0.5}Mn_{1.5}O_4$ cathode materials for 5 V lithium ion batteries [J]. Applied Surface Science, 2014, 290: 412−418.

[17] KIM Jung-hyun, PIECZONKA N P W, SUN Yang-kook, POWELL B R. Improved lithium-ion battery performance of $LiNi_{0.5}Mn_{1.5-x}Ti_xO_4$ high voltage spinel in full-cells paired with graphite and $Li_4Ti_5O_{12}$ negative electrodes [J]. Journal of Power Sources, 2014, 262: 62−71.

[18] KIZILTAS-YAVUZ N, BHASKAR A, DIXON D, YAVUZ M, NIKOLOWSKI K, LU Li, EICHEL R A, EHRENBERG H. Improving the rate capability of high voltage lithium-ion battery cathode material $LiNi_{0.5}Mn_{1.5}O_4$ by ruthenium doping [J]. Journal of Power Sources, 2014, 267: 533−541.

[19] MAO Jing, MA Meng-ze, LIU Pan-pan, HU Jun-hua, SHAO Guo-sheng, BATTAGLIA V, DAI Ke-hua, LIU Gao. The effect of cobalt doping on the morphology and electrochemical performance of high-voltage spinel $LiNi_{0.5}Mn_{1.5}O_4$ cathode material [J]. Solid State Ionics, 2016, 292: 70−74.

[20] WANG Wei, LIU Heng, WANG Yan, GAO Chao, ZHANG Jun. Effects of chromium doping on performance of $LiNi_{0.5}Mn_{1.5}O_4$ cathode material [J]. Transactions of Nonferrous Metals Society of China, 2013, 23: 2066−2070.

[21] LIU Hai-dong, WANG Jun, ZHANG Xiao-fei, ZHOU Dong, QI Xin, QIU Bao, FANG Jian-hui, KLOEPSCH R, SCHUMACHER G, LIU Zhao-ping, LI Jie. Morphological evolution of high-voltage spinel $LiNi_{0.5}Mn_{1.5}O_4$ cathode materials for lithium-ion batteries: The critical effects of surface orientations and particle size [J]. ACS Applied Materials Interfaces, 2016, 8: 4661−4675.

[22] WANG Jing, LIN Wei-qing, WU Bi-he, ZHAO Jin-bao. Syntheses and electrochemical properties of the Na-doped $LiNi_{0.5}Mn_{1.5}O_4$ cathode materials for lithium-ion batteries [J]. Electrochimica Acta, 2014, 145: 245−253.

[23] KIM J H, MYUNG S T, YOON C S, KANG S G, SUN Y K. Comparative study of $LiNi_{0.5}Mn_{1.5}O_{4-\delta}$ and $LiNi_{0.5}Mn_{1.5}O_4$ cathodes having two crystallographic structures: $Fd3m$ and $P4_332$ [J]. Chemistry of Materials, 2004, 16: 906−914.

[24] STROBEL P, IBARRA-PALOS A, ANNE M, LE CRAS F. Structural, magnetic and lithium insertion properties of spinel-type $Li_2Mn_3MO_8$ oxides (M=Mg, Co, Ni, Cu) [J]. Journal of Materials Chemistry, 2000, 10: 429−436.

[25] ZHONG Qi-ming, BONAKDARPOUR A, ZHANG Mei-jie, GAO Yuan, DAHN J R. Synthesis and electrochemistry of $LiNi_xMn_{2-x}O_4$ [J]. Journal of the Electrochemical Society, 1997, 144: 205−213.

[26] WANG Li-ping, LI Hong, HUANG Xue-jie, BAUDRIN E. A comparative studyof Fd-$3m$ and $P4_332$ "$LiNi_{0.5}Mn_{1.5}O_4$" [J]. Solid State Ionics, 2011, 193: 32−38.

[27] SONG Jie, SHIN D W, LU Yu-hao, AMOS C D, MANTHIRAM A, GOODENOUGH J B. Role of oxygen vacancies on the performance of $Li[Ni_{0.5-x}Mn_{1.5+x}]O_4$ (x=0, 0.05, and 0.08) spinel cathodes for lithium-ion batteries [J]. Chemistry of Materials, 2012, 24: 3101−3109.

[28] CABALLERO A, CRUZ M, HERNÁN L, MELERO M, MORALES J, RODRÍGUEZ CASTELLÓN E. Oxygen deficiency as the origin of the disparate behavior of $LiM_{0.5}Mn_{1.5}O_4$ (M=Ni, Cu) nanospinels

in lithium cells [J]. Journal of the Electrochemical Society, 2005, 152: A552−A559.

[29] XIAO Jie, CHEN Xi-lin, SUSHKO P V, SUSHKO M L, KOVARIK L, FENG Ji-jun, DENG Zhi-qun, ZHENG Jian-ming, GRAFF G L, NIE Zi-min, CHOI D, LIU Jun, ZHANG Ji-guang, WHITTINGHAM M S. High-performance $LiNi_{0.5}Mn_{1.5}O_4$ spinel controlled by Mn^{3+} concentration and site disorder [J]. Advanced Materials, 2012, 24: 2109−2116.

[30] GAO Po, WANG Lu, CHEN Lin, JIANG Xue-fan, PINTO J, YANG Gang. Microwave rapid preparation of $LiNi_{0.5}Mn_{1.5}O_4$ and the improved high rate performance for lithium-ion batteries [J]. Electrochimica Acta, 2013, 100: 125−132.

[31] BAO Shu-juan, LI Chang-ming, LI Hu-lin, LUONG J H T. Morphology and electrochemistry of $LiMn_2O_4$ optimized by using different Mn-sources [J]. Journal of Power Sources, 2007, 164: 885−889.

[32] IDEMOTO Y, NARAI H, KOURA N. Crystal structure and cathode performance dependence on oxygen content of $LiMn_{1.5}Ni_{0.5}O_4$ as a cathode material for secondary lithium batteries [J]. Journal of Power Sources, 2003, 119−121: 125−129.

[33] KUNDURACI M. AMATUCCI G G. Synthesis and characterization of nanostructured 4.7V $Li_xMn_{1.5}Ni_{0.5}O_4$ spinels for high-power lithium-ion batteries [J]. Journal of the Electrochemical Society, 2006, 153: A1345−A1352.

[34] ALCÁNTARA R, JARABA M, LAVELA P, TIRADO J L, ZHECHEVA E, STOYANOVA R. Changes in the local structure of $LiMg_yNi_{0.5-y}Mn_{1.5}O_4$ electrode materials during lithium extraction [J]. Chemistry of Materials, 2004, 16: 1573−1579.

[35] KUNDURACI M, AL-SHARAB J F, AMATUCCI G G. High-power nanostructured $LiMn_{2-x}Ni_xO_4$ high-voltage lithium-ion battery electrode materials: Electrochemical impact of electronic conductivity and morphology [J]. Chemistry of Materials, 2006, 18: 3585−3592.

[36] ARIYOSHI K, IWAKOSHI Y, NAKAYAMA N, OHZUKU T. Topotactic two-phase reactions of $Li[Ni_{1/2}Mn_{3/2}]O_4$ ($P4_332$) in nonaqueous lithium cells [J]. Journal of the Electrochemical Society, 2004, 151: A296−A303.

[37] LIU D, ZHU W, TROTTIER J, GAGNON C, BARRAY F, GUERFI A, MAUGER A, GROULT H, JULIEN C M, GOODENOUGH J B, ZAGHIB K. Spinel materials for high-voltage cathodes in Li-ion batteries [J]. RSC Advances, 2014, 4: 154−167.

[38] FANG Hai-sheng, WANG Zhi-xing, ZHANG Bao, LI Xin-hai, LI Guang-she. High performance $LiNi_{0.5}Mn_{1.5}O_4$ cathode materials synthesized by a combinational annealing method [J]. Electrochemical Communications, 2007, 9: 1077−1082.

[39] SHIN D W, BRIDGES C A, HUQ A, PARANTHAMAN M P, MANTHIRAM A. Role of cation ordering and surface segregation in high-voltage spinel $LiMn_{1.5}Ni_{0.5-x}M_xO_4$ (M=Cr, Fe, and Ga) cathodes for lithium-ion batteries [J]. Chemistry of Materials, 2012, 24: 3720−3731.

[40] LIU Zu-shan, JIANG Yang-mei, ZENG Xiao-yuan, XIAO Guan, SONG Hui-yu, LIAO Shi-jun. Two-step oxalate approach for the preparation of high performance $LiNi_{0.5}Mn_{1.5}O_4$ cathode material with high voltage [J]. Journal of Power Sources, 2014, 247: 437−443.

[41] CHEMELEWSKI K R, MANTHIRAM A. Origin of site disorder and oxygen nonstoichiometry in $LiMn_{1.5}Ni_{0.5-x}M_xO_4$ (M=Cu and Zn) cathodes with divalent dopant ions [J]. The Journal of Physical Chemistry C, 2013, 117: 12465−12471.

[42] STROBEL P, IBARRA-PALOS A, ANNE M, POINSIGNON C, CRISCI A. Cation ordering in $Li_2Mn_3MO_8$ spinels: Structural and vibration spectroscopy studies [J]. Solid State Science, 2003, 5: 1009−1018.

[43] JIN Yi-chun, LIN Chih-yuan, DUH Jenq-gong. Improving rate capability of high potential $LiNi_{0.5}Mn_{1.5}O_{4-x}$ cathode materials via increasing oxygen non-stoichiometries [J]. Electrochimica Acta, 2012, 69: 45−50.

[44] SHA Ou, TANG Zhi-yuan, WANG Shao-liang, YUAN Wei, QIAO Zhi, XU Qiang, MA Li. The multi-substituted $LiNi_{0.475}Al_{0.01}Cr_{0.04}Mn_{1.475}O_{3.95}F_{0.05}$ cathode material with excellent rate capability and cycle life [J]. Electrochimica Acta, 2012, 77: 250−255.

[45] WANG Hai-long, TAN T A, YANG Ping, LAI M O, LU Li. High-rate performances of the Ru-doped spinel $LiNi_{0.5}Mn_{1.5}O_4$: Effects of doping and particle size [J]. The Journal of Physical Chemistry C, 2011, 115: 6102−6110.

[46] CHEMELEWSKI K R, LEE Eun-sung, LI Wei, MANTHIRAM A. Factors influencing the electrochemical properties of high-voltage spinel cathodes: Relative impact of morphology and cation ordering [J]. Chemistry of Materials, 2013, 25: 2890−2897.

[47] ZHONG G B, WANG Y Y, YU Y Q, CHEN C H. Electrochemical investigations of the $LiNi_{0.45}M_{0.10}Mn_{1.45}O_4$ (M=Fe, Co, Cr) 5 V cathode materials for lithium ion batteries [J]. Journal of Power Sources, 2012, 205: 385−393.

[48] JAFTA C J, MATHE M K, MANYALA N, ROOS W D, OZOEMENA K I. Microwave-assisted synthesis of high-voltage nanostructured $LiMn_{1.5}Ni_{0.5}O_4$ spinel: Tuning the Mn^{3+} content and electrochemical performance [J]. ACS Applied Materials Interfaces, 2013, 5: 7592−7598.

[49] DUNCAN H, HAI Bin, LESKES M, GREY C P, CHEN Guo-ying. Relationships between Mn^{3+} content, structural ordering, phase transformation, and kinetic properties in $LiNi_xMn_{2-x}O_4$ cathode materials [J]. Chemistry of Materials, 2014, 26: 5374−5382.

[50] HAI Bin, SHUKLA A K, DUNCAN H, CHEN Guo-ying. The effect of particle surface facets on the kinetic properties of $LiMn_{1.5}Ni_{0.5}O_4$ cathode materials [J]. Journal of Materials Chemistry A, 2013, 1: 759−769.

[51] CAI Yi, HUANG Shao-zhuan, SHE Fa-shuang, LIU Jing, ZHANG Run-lin, HUANG Zhen-hong, WANG Feng-yun, WANG Hong-en. Facile synthesis of well-shaped spinel $iNi_{0.5}Mn_{1.5}O_4$ nanoparticles as cathode materials for lithium ion batteries [J]. RSC Advances, 2016, 6: 2785−2792.

[52] LIU Jian-zhong, NI Jiang-feng, ZHAO Yang, WANG Hai-bo, GAO Li-jun. Grapecluster-like Fe_3O_4@C/CNT nanostructures with stable Li-storage capability [J]. Journal of Materials Chemistry A, 2013, 1: 12879−12884.

[53] NI Jiang-feng, ZHOU Heng-hui, CHEN Ji-tao, ZHANG Xin-xiang. Molten salt synthesis and electrochemical properties of spherical $LiFePO_4$ particles [J]. Materials Letters, 2007, 61: 1260−1264.

[54] CHENG Fang-yi, WANG Hong-bo, ZHU Zhi-qiang, WANG Yan, ZHANG Tian-ran, TAO Zhan-liang, CHEN Jun. Porous $LiMn_2O_4$ nanorods with durable high-rate capability for rechargeable Li-ion batteries [J]. Energy & Environmental Science, 2011, 4: 3668−3675.

[55] CUI Yan, ZHAO Xiao-li, GUO Rui-song. High rate electrochemical performances of nanosized ZnO and carbon co-coated $LiFePO_4$ cathode [J]. Materials Research Bulletin, 2010, 45: 844−849.

[56] FANG Hai-sheng, YI Hui-hua, HU Cheng-lin, YANG Bin, YAO Yao-chun, MA Wen-hui, DAI Yong-nian. Effect of Zn doping on the performance of $LiMnPO_4$ cathode for lithium ion batteries [J]. Electrochimica Acta, 2012, 71: 266−269.

[57] CUI Yan, ZHAO Xiao-li, GUO Rui-song. Improved electrochemical performance of $La_{0.7}Sr_{0.3}MnO_3$ and carbon co-coated $LiFePO_4$ synthesized by freeze-drying process [J]. Electrochimica Acta, 2010, 55: 922−926.

Na^+掺杂对锂离子电池正极材料 $LiNi_{0.5}Mn_{1.5}O_4$晶体结构和电化学性能的影响

王江峰，陈 丹，吴 伟，王 丽，梁广川

河北工业大学 能源与环保材料研究所 生态环境与信息特种功能材料教育部重点实验室，天津 300130

摘 要：采用简单固相法制备 $LiNi_{0.5}Mn_{1.5}O_4$ 及 Na^+掺杂的 $Li_{0.95}Na_{0.05}Ni_{0.5}Mn_{1.5}O_4$ 正极材料，研究 Na^+掺杂对 $LiNi_{0.5}Mn_{1.5}O_4$ 材料晶体结构和电化学性能的影响。分别采用 XRD、SEM、FT-IR、CV、EIS 和恒流充放电测试对样品进行表征。结果表明，未掺杂和 Na^+掺杂样品均为由八面体一次颗粒组成的二次团聚体颗粒，Na^+掺杂在一定程度上减小了一次颗粒尺寸。Na^+掺杂可有效抑制 $Li_xNi_{1-x}O$ 杂相的生成，提高 Ni/Mn 无序度，降低电荷转移阻抗，加快锂离子扩散，从而提高材料的倍率性能。但是，掺杂的 Na^+倾向占据锂离子的 8*a* 位置，从而迫使相同数量的锂离子占据 16*d* 八面体位置，这使尖晶石结构变得不稳定，因此，Na^+掺杂并没有改善 $LiNi_{0.5}Mn_{1.5}O_4$ 材料的循环稳定性。

关键词：正极材料；$LiNi_{0.5}Mn_{1.5}O_4$；Na^+掺杂；电化学性能

(Edited by Bing YANG)